Duple extinguishment of COVID-19: single compound synergized inhibition of SARS-CoV-2 replication and direct suppression of inflammatory cytokines *in vitro/vivo*

Authors: Zhesheng He[2†], Fei Ye[3†], Zhongying Du[1], Chunyu Zhang[1], Wencong Zhao[1], Yucong Gao[6], Qing Yuan[1], Fuping Gao[2], Yuhui Dong[2], Jiadong Fan[4], Bo He[4], Peng Cao[5], Xuejiao Gao[8], Xingfa Gao[8], Bo Sun[9], Jicun Zhao[10], Jianxun Qi[7], Huaidong Jiang[4], Wenjie Tan[3]*, Yong Gong[2*], Xueyun Gao[1]*

Affiliations:
[1]Beijing University of Technology, Ping Le Yuan 100, Beijing, P. R. China.
[2]Institute of High Energy Physics, Chinese Academy of Sciences, Beijing 100049, P. R. China.
[3]Key Laboratory of Biosafety, National Health and Family Planning Commission, National Institute for Viral Disease Control and Prevention, China CDC, Beijing102206, P. R. China.
[4]Shool of physical science and technology, ShanghaiTech University, Shanghai 201210, P. R. China.
[5]National Laboratory of Biomacromolecules, Institute of Biophysics, Chinese Academy of Sciences, Beijing 100101, P. R. China.
[6]College of Engineering Civil, Environmental and Geodetic Engineering, The Ohio State University, Columbus, OH 43210, USA.
[7]CAS Key Laboratory of Pathogenic Microbiology and Immunology, Institute of Microbiology, Chinese Academy of Sciences, Beijing 100101, P. R. China.
[8]College of Chemistry and Chemical Engineering, Jiangxi Normal University, Nanchang 330022, P. R. China.
[9]Shanghai Advanced Research Institute, Chinese Academy of Sciences, No.239 Zhangheng Road, Shanghai, China, 201204.
[10]State Key Laboratory of Respiratory Disease, National Clinical Research Center for Respiratory Disease, Guangzhou Institute of Respiratory Health, First Affiliated Hospital of Guangzhou Medical University, Guangzhou, China

[†]These authors contributed equally to this work.

*Correspondence to: Xueyun Gao (gaoxy@ihep.ac.cn)

One Sentence Summary: Single gold compound not only significantly inhibits SARS-CoV-2 replication in lung and but also directly suppress lung inflammatory injury in COVID-19 mice, it is with great potential to effectively treat COVID-19.

Abstract:

The virus replication and lung inflammation are basic targets for COVID-19 treatment. To effectively treat COVID-19, the best chemical drug should combine inhibition of SARS-CoV-2 replication and direct suppression of inflammatory cytokine expression together. Our SARS-CoV-2 main protease (M^{pro}) crystal structure studies revealed Au(I), derived from auranofin (AF) or gold cluster (GA), could specifically bind thiolate of Cys145 of SARS-CoV-2 M^{pro}. GA or AF could well inhibit M^{pro} activity and significantly decrease SARS-CoV-2 replication in cell. Cell studies showed that either AF or GA could down-regulate NFκB pathway, therefore significantly inhibit inflammatory cytokine level of IL-6, IL-1β, TNF-α in macrophage and bronchial epithelial cell, respectively. The lung viral load in GA treated COVID-19 mice (15mg/kg.bw) is significantly lower than that in normal saline (NS, 0.9% NaCl) treated COVID-19 mice, and pathological studies revealed GA treatment (score ~1.8) significantly reduced lung inflammatory injury compared with NS treated COVID-19 mice (score ~3). After normal mice were treated by GA (15mg/kg), the Au ingredient well distributed into lungs and there are no pathological changes in main organs when compared with control mice. The toxicity results revealed GA is more safety than auranofin for cell/mice/rat. The rat pharmacokinetics studies show GA is with high bioavailability (> 90%) *in vivo*.

Main Text:

The COVID-19 pandemic is threatening human in the world now. There are more than 30 million COVID-19 patients and over 1 million of them were dead by the end of September 2020. To date, there are no drugs to effectively treat this disease. Until now, the drug screening strategy has mainly focused on identifying antibodies that can perfectly block key proteins of SARS-CoV-2 to inhibit virus replication or well suppress inflammatory cytokines level to decrease lung injury (*1*, *2*). In principle, chemical drugs are of unique advantages in dealing with the COVID-19 pandemic: the chemical drugs are easily produced in large scale with low cost thus satisfy the huge amount of COVID-19 patients of low income in the world, and they can be easily handled, stored and distributed to the patients living in various natural and social environment. Now, several traditional chemical drugs are being used to treat COVID-19, but they have been far from satisfying in treatment of COVID-19 in clinic (*3*, *4*, *5*, *6*, *7*, *8*). For example, Remdesivir could inhibit SARS-CoV-2 replication but couldn't directly suppress the inflammatory cytokines level and protect lung from inflammation injury in severe patients (*4*, *8*), and Ruxolitinib and Acalabrutinib could directly suppress inflammatory cytokines level to save severe patients' life but could not inhibit virus replication to help patients quickly recover (*5*, *7*).

We propose a new concept of chemical drug treating COVID-19: a single drug not only directly suppresses inflammatory cytokines level but also inhibits SARS-CoV-2 replication, such drug would synergize two therapy effects to produce more promising outcome for COVID-19 treatment. US FDA has approved AF to treat amebiasis as orphan-drug and to treatment Rheumatoid arthritis (RA), respectively. There are no reports to disclose gold compounds could treat COVID-19 *in vivo*, neither to reveal how these compounds work in molecular/cellular level

to against COVID-19. We speculate gold compounds are potential candidates to fulfill the aforementioned new concept chemical drugs. **Firstly**, we are with insight that gold compounds might inhibit SARS-CoV-2 replication *via* directly targeting the thiolate of Cys145 of M^{pro} of COVID-19. It is known that M^{pro} is a chemical drug target as it plays a key role in SARS-CoV-2 replication. Many compounds have been screened to interact with the thiolate of Cys145 as it is the conserved residue of the catalytic dyad of M^{pro} (*9, 10*). Previous reports and our published papers both discussed the Au(I) ions derived from gold compounds could inactivate kinds of enzyme by directly interacting their key Cys residues in *vitro/vivo* (*11, 12, 13, 14, 15, 16, 17*). **Secondly**, gold compounds are widely known to inhibit inflammatory cytokines associated with rheumatoid arthritis (RA), thus they have the potential to counter the inflammation in COVID-19 (*2, 5, 7*). For example, Auranofin (AF) is FDA approved drug for treating RA (*11, 12, 13, 16*) and it can well suppress inflammatory cytokines of IL-6, IL-1β, TNF-α in RA patients. AF has the potential to treat COVID-19 because these inflammatory cytokines play an important role in lung injury of severe patients (*2, 5, 7*). However, AF has severe side effects for RA patients. Recently, we have disclosed a gold compound, the gold cluster (GA), which produces very good outcome in RA treatment and is more safety comparing with AF (*14, 15, 18*). In the present study, we verify AF or GA could treat COVID-19 via synergy the direct suppression inflammatory cytokine level and inhibit SARS-CoV-2 replication *in vitro/vivo*.

Results

Crystal structure of SARS-CoV-2 M^{pro} complex with Au(I) derived from AF or GA

In order to examine the structural basis of AF and GA activities in more details, we determined the SARS-CoV-2 M^{pro} crystal structures in the AF incubating form, the GA incubating form, and

the native form (**Figure 1, Figure S3, S4, and Table S1**). Generally speaking, the M^{pro} structures treated with the gold compounds have a high similarity, and they are all similar to the crystal structures of the apo SARS-CoV-2 M^{pro} determined most recently (*9, 10*). However, in the AF or GA treated structures, densities of two Au(I) ions were found clearly to be near to the thiol residues Cys145 and Cys156, which were confirmed by the anomalous difference Fourier maps (**Figure 1B and Figure S3b, S3c**). They are defined as Au(I) 1 and Au(I) 2, respectively. This suggests that the AF or GA can provide Au(I) ions which bind to the thiolate of Cys145 and Cys156 of M^{pro} protein *via* Michael addition reactions (*17*). The overall structure of Au(I)-M^{pro} complex presents a homodimeric form (**Figure 1A**), with each monomer comprising three main domains (**Figure 1B**), like the SARS-CoV-2 M^{pro} reported previously (*9, 10*). Domains I and II are β-barrels, which together resemble the chymotrypsin structure with the active site located in a cleft between them, whereas domain III are mainly composed of α-helices. The Au(I) 1 is in the active pocket of the M^{pro}, and it is coordinated by the S atom of Cys145 (**Figure 1B, 1C**), which is the key conserved residue contributing to the catalytic dyad. The Au(I) 2 is at the outer area of M^{pro} and is coordinated by the S atom of Cys156 (**Figure 1B**). Temperature factor analysis shows that the occupancy of two Au(I) ions is partial, indicating that the Au(I) ions are introduced into the M^{pro} gradually from AF or GA.

Comparison of the state of Au(I)-M^{pro} with the native state of M^{pro} shows the introduction of Au(I) does not induce the obvious M^{pro} conformational change (**Figure 1C)**. The Au(I) 1 ion specifically binds to the conserved Cys145 and it is trapped in the active pocket (**Figure 1C**), indicating that it can block the active site and inhibit the catalytic function of the key residues of the catalytic dyad. For AF or GA treated M^{pro}, the distances between the Cys145 and Au(I) is 2.2Å and 2.3Å ,respectively. Such a short bond length confirms that the Au(I) covalently binds

to S atom of Cys145 (**Figure 1C, Figure S3**). Once Au(I) bonds the Cys145, the distance between the catalytic dyad Cys145 and His41 change from 3.7Å to 3.9Å (**Figure 1C**). Although there are 12 Cys residues in M^{pro} monomer (Cys16, Cys22, Cys38, Cys44, Cys85, Cys117, Cys128, Cys145, Cys156, Cys160, Cys265, Cys300), only Cys145 and Cys156 specifically bind to the Au(I). To further verify Au(I) ions covalently binding to the S atom of Cys145 and Cys156, the interaction energies between Au and M^{pro} protein were calculated by density functional theory (DFT) methods. The bond dissociation energies (E_{BD}'s) between Au(I) and M^{pro} are 46.1 kcal mol−1 for Cys145 and 26.5 kcal mol^{-1} for Cys156, respectively (**Figure 1D**). Such large E_{BD}'s suggest that the Au atoms firmly bind to Cys145 and lock the active pocket of M^{pro}, which efficiently inhibit the catalytic activity.

AF or GA inhibited SARS-CoV-2 M^{pro} activity, suppress SARS-CoV-2 replication and inhibit inflammatory cytokine expression in cell

To exam whether AF or GA can well inhibit M^{pro} activity. The IC50 of AF or GA was determined *via* the reported method (*19*). In order to characterize M^{pro} activity, we used a fluorescence resonance energy transfer (FRET) assay. To do this, a fluorescence labeled substrate, (EDNAS-Glu)-Ser-Ala-Thr-Leu-Gln-Ser-Gly-Leu-Ala-(Lys-DABCYL)-Ser, derived from the auto-cleavage sequence of the viral protease was chemically modified for enzyme activity assay. For inhibiting M^{pro} activity *in vitro*, IC50 of AF is ~0.46 μM **(Figure 2A**) and that of GA is ~3.30 μM (**Figure 2B**), respectively. Compared with the IC50 of reported compounds (0.67μM for Ebselen), AF shows very strong ability to inhibit M^{pro} i*n vitro* (*9*, *10*).

We further studied the EC50 of AF or GA to see if these gold compounds could significantly inhibit SARS-CoV-2 replication in Vero cell in the Biosafety Level-3 Lab of China CDC *via* the

following reported methods (*6*). The EC50 of AF is ~0.83 μM (**Figure 2C**) and that of GA is ~7.32μM (**Figure 2D**), respectively. The EC50 of FA is very close to that of Remdesivir in SARS-CoV-2 infected Vero cell (*6*). Recently, Mukesh Kumar et al. reported that AF could well inhibit SARS-CoV-2 replication in infected Huh cell and the EC50 of AF was ~1.4 μM, and they explained that inhibition of SARS-CoV-2 replication may be induced by gold compound suppressing the thioredoxin reductase activity and inducing ER stress of host cell (*20*). Based on our crystal structure studies and M^{pro} activity data, we believe that gold compounds inhibit SARS-CoV-2 replication *via* Au(I) binding to Cys145 of M^{pro} and further suppressing it activity in host cell.

Most recently, a clinical study revealed that severe COVID-19 patients have a hyper-inflammatory immune response associated with macrophage activation (*5*). By using the RA treatment drugs, Ruxolitinib, to inhibit the activation of NFκB pathway in macrophages, down-regulation of the expression level of IL-6, IL-1β, TNF-α were acquired and the oxygenation and clinical status of most severe patients on supplemental oxygen improved relatively rapidly. This clinical study matches viewpoints of the recent review papers (*21, 22, 23, 24, 25*). To further verify the fact that AF or GA can well inactivate NFκB in macrophage cells and further down-regulate expression of IL-6, IL-1β, TNF-α cytokine therein, the macrophage line RAW264.7 were cultured and incubated with a serial dose of AF or GA for 24 hours, respectively. The low dose of AF (1.2 μM) significantly suppressed IL-6, IL-1β and TNF-α expression levels in the macrophages (**Figure 2E**). GA of high dose (40μM) significantly suppressed inflammatory macrophage producing IL-6, IL-1β, TNF-α (**Figure 2E**). In inflammatory macrophages, the nuclear factor NFκB is the key signaling pathways that regulate the inflammatory mediator genes. Inflammatory factors can induce the activation of the IκB kinase (IKK) complex, cause

subsequent degradation of IκB proteins, and release p-p65 which enters the nuclei to induce the expression of TNF-α, IL-1β and IL-6. In **Figure 2E**, AF or GA treatment could well decrease IKK phosphorylation level, this further suppressed IκB phosphorylation and inhibit p65 phosphorylation. AF of low dose (1.2 μM) could well inhibit phosphorylation of IKK, IκB, and p65, thus suppress the NFκB activation (**Figure 2E**). In contrast, GA of high dose (40 μM) could significantly inhibit phosphorylation of IKK, IκB, and p65, thus suppress NFκB activation in inflammatory macrophage (**Figure 2E**). For COVID-19, virus infected bronchial epithelial cell would activate NFκB pathway to express inflammatory cytokine, these cytokines will activate macrophage into inflammatory status (*22, 23, 24*). We also carried studies to verify gold compound could inactivate NFκB pathway and suppress inflammatory cytokine express level in inflammatory human bronchial epithelial cells (**Figure 2F**). AF in low dose of (0.15μM) and GA of high dose (20 μM) could significantly inhibit phosphorylation level of IKK, IκB, p65 to suppress NFκB activation, thus well inhibit IL-6, IL-1β, and TNF-αinflammatory cytokine expression in cell **(Figure 2F)**. Although the aforementioned data showed AF is more active to suppress inflammatory cytokine in cell studies. However, previous reports revealed that GA (5 mg/kg.bw) could well treat RA when compared with auranofin (6 mg~9 mg/kg.bw) (*11, 12, 14, 15*), this implied that the therapy efficiency is similar when AF and GA applied in RA treatment *in vivo* even they show significant different potency in cell studies.

The toxicity study of AF or GA compounds in vitro/vivo

As the safety features of AF or GA are key parameter for their later animal studies, we firstly checked the gold compounds' toxicity in Vero E6 cell, bronchial epithelial cells, and macrophages as these cells play key role in SARS-CoV-2 replication and inflammatory cytokine production, respectively (5, *6, 22, 23, 24*). For human bronchial epithelial cells (16HBE), CC50

of AF is about ~0.6 μM while the GA shows no cell toxicity even at a concentration of 100 μM in cell culture media for 48 hrs (**Table 1** and **Figure S5a**). For Vero E6 cell, CC50 of AF is about ~2.2 μM and GA show none cell toxicity when 100 μM gold clusters were introduced in cell culture media for 48 hrs (**Table 1** and **Figure S5b**). And for macrophages (RAW264.7), CC50 of AF is about ~2.4 μM and GA show no cell toxicity when its dose increased to 100 μM in cell culture media for 48 hrs (**Table 1** and **Figure S5c**). For mice acute toxicity, the intraperitoneal LD50 for AF is about ~33.8 mg/kg (*26*), and that for GA is over ~1000 mg/kg (none mice dead, see **Supplementary Materials** for detail). For rat acute toxicity, the intraperitoneal LD50 for AF is ~25.5 mg/kg and that for GA is about ~288 mg/kg.bw (*14*, *26*). For rat/mice RA treatment, oral AF in dose of 6~9 mg/kg.bw and intraperitoneal injection GA at 5 mg/kg.bw both significantly suppress inflammatory cytokine level and get similar outcome to RA rat/mice (*13, 14, 15, 16*). The aforementioned cell, mice and rat toxicity, and RA mice/rat treatment data all imply that GA are more safety than AF when consider their treatment COVID-19 *in vivo*.

GA significantly suppress SARS-CoV-2 replication in lung and protect lung from inflammatory injury in COVID-19 mice model

The COVID-19 mice model was generated following recently reported method and detailed procedures are illustrated in **Figure 3A** (*27*). Briefly, twelve BLAC/C mice were divided into 3 groups, mice were anesthetized with pentasorbital sodium and transduced intranasally with 2.5×10^8 FFU of Ad5-ACE2 in 50 μL DMEM. Five days post transduction, the mice received a dose of 15 mg/kg.bw GA via intraperitoneal injection (i.p.) 1 hour before SARS-CoV-2 infection. An equivalent volume of normal saline (NS, 0.9% NaCl) was administered as a control. Then mice were infected intranasally with SARS-CoV-2 (1×10^5 PFU) in a total volume

of 50 μL DMEM. After virus infection at day 0, mice received GA or NS treatment for three time as illustrated in **Figure 3A**. All mice were euthanized at day 4 and the body weight loss, SARS-CoV-2 RNA copies in lung, lung pathological change, key inflammatory cytokine level (IL-6, IL-1β, TNF-α) in lung were studied.

The COVID-19 mice model was successfully produced. In the SARS-COV-2 infected mice treated by NS, significant body weight loss (**Figure 3B**), higher SARS-CoV-2 RNA copies in lung (**Figure 3C**), and severe bronchopneumonia and interstitial pneumonia and infiltration of lymphocytes within alveolar were clearly observed (**Figure 3D**). The pathological scores of mice lung tissue were assessed by grading the injury from 0 to 4 in accordance with the INHAND scoring standard, the average pathological score of virus infected mice treated by NS is about ~3 (**Figure 3E**). The body weight loss of GA treated mice was slighter when compared with that of NS treated COVID-19 mice (**Figure 3B**). The number of viral RNA copies in lung of GA treated mice was with about ~$4\times\log10^4$, it was significant lower than the NS treated infected mice ~$5\times\log10^5$ (**Figure 3C**). We further evaluate the therapeutic effect through a histopathological analysis of lung tissue of the mice. The SARS-CoV-2 infected mice treated with NS showed severe lung inflammation. The alveolar septum, bronchus, bronchioles and perivascular interstitium were significantly widened, along with more lymphocytes and a small number of neutrophils infiltrated. Also, a small number of lymphocytes and exfoliated epithelial cells were found in the lumen of local bronchioles of NS treated mice (**Figure 3E, Figure S6**). Treatment with GA abrogated the characteristic signs of lung inflammation in SARS-CoV-2 infected mice. Local alveolar septum, bronchi, bronchiole and perivascular interstitial widening significantly decreased. Although there was still some lymphocytic infiltration, the mucosal epithelium of bronchus and bronchioles was intact, and there was no foreign body in the lumen, which was

comparable to lung tissue sections of the mock mice that were not infected by the SARS-CoV-2. In **Figure 3D**, the mean pathological score obtained from histopathological lung observation further demonstrated that GA significantly ($p < 0.001$) reduced pathological scores (~1.8) compared with those of SARS-CoV-2 infected mice treated with NS (~3.0). The inflammatory cytokines in lung of the mice were shown by immuno-fluoresce imaging, and the IL-6, IL-1β, TNF-α express level in lung of GA treated mice was lower than that of NS treated mice. The GA treatment of COVID-19 mice significantly protect lung from injury *via* inhibiting virus replication and suppressing the inflammatory cytokine expression in SARS-CoV-2 infected mice.

The bio-distribution, tissue pathologic, and pharmacokinetic studies of GA in mice/rat

In aforementioned COVID-19 model study, BLAC/C mice were treated with GA in dose of 15 mg/kg.bw for 4 times. To check the tissue distribution of Au ingredient and see if Au ingredient induced tissue side effects, six normal BLAC/C mice in the treatment group were intraperitoneally injection of 15mg/kg.bw GA 4 times for 1 time/day, and the mice in the control group were injected with NS in same way. During this study, we didn't observe any side effects in the GA treated mice on aspects of movement, outlooking, sleeping, and eating behaviors. The pathological images of mouse brains, hearts, livers, lungs, spleens, and kidneys were showed in. For mouse tissue sections dyed by Hematoxylin-eosin (HE), no pathological change was found when compared GA with NS treated mice, which implied 15mg/kg.bw GA treatment is safe for mice in this study (*18*). The Au ingredient distribution in mice organs was analysis by ICP-MASS and the result shown in **Table 2.** In lung, the Au element concentration is ~51.07μg/g, which accountable for GA inhibiting virus replication and suppressing inflammatory cytokine

level therein. The gold ingredient distribution in hearts, livers, kidneys, brains, and spleens can be beneficial for COVID-19 treatment as they can potentially inhibit SARS-CoV-2 replication and suppression inflammation cytokine level therein. As shown in **Table 2**, the Au ingredient mainly concentrated on spleen, heart, and kidney. The high level of Au in kidney implied the Au ingredient may quickly excrete via urine, this is consistent with the following pharmacokinetics data of GA in rat model (**Table 3**).

When gold compounds are applied in later preclinical animal studies to against COVID-19, the pharmacokinetics parameter should be clarified firstly. The pharmacokinetics study of gold cluster via intraperitoneal injection rat was shown in **Table 3**. After rats are intraperitoneally injected 5 mg/kg.bw of GA for one time, Au concentration of plasma was tested in different time point and kinetic characteristics of gold cluster in rats were analyzed. According to the calculated parameters, the values of T_{max} for GA in male or female rats were 2 hours and the values of C_{max} for GA in male or female rats were 29.99μg/mL or 31.750μg/mL, respectively. The values of $t_{1/2z}$ for GA in male or female rats were 21.626 hr or 11.068 hr, respectively. Combine the data analysis of intravenous injection of GA at 5 mg/kg.bw (**Table S2**), the F values of bioavailability (**Table 3**) for GA in male or female rats were 92.06% or 96.41%, respectively. These data confirmed that GA has favorable bioavailability *in vivo.*

Discussion

Gold compounds have been developed for diseases treatment in long history. US FDA has approved AF to treatment RA disease and to treat amebiasis, respectively, although it is with severe side effects for patients (*11*, *27*). However, there are no reports to disclose whether gold compounds could treat COVID-19 or not *in vivo*. Our studies firstly revealed that Au(I) derived

from AF or GA can specifically bind to thiolate of Cys145 of SARS-CoV-2 M^{pro} although there are 12 free Cys residues in M^{pro} monomer (*9,10*). As Cys145 is the conserved residue of the catalytic dyad of M^{pro}, such Au(I)-Cys145 binding significantly suppress M^{pro} activity. Because M^{pro} plays key role in virus replication, therefore AF or GA could significantly inhibit SARS-CoV-2 replication in cell. In addition, AF or GA could significantly down-regulate NFκB activation and further decrease inflammation cytokine expression level of IL-6, IL-1β and TNF-α in macrophages and human bronchial epithelial cells, respectively. The COVID-19 mice model studies showed that GA effectively inhibited SARS-COV-2 replication in lung and significantly protected lung from inflammation injury, and body weight loss of COVID-19 mice were obviously suppressed via GA treatment. The mice/rat acute toxicity studies revealed GA is more safety than AF *in vivo*. The pharmacokinetics data confirmed that GA has favorable bioavailability, over 90%, GA metabolism well distributed in lung and other organs but has not induced pathological changes of these organs. Now, the GA is under further preclinical COVID-19 studies.

References and Notes:

1. S. Du, Y. Cao, Q. Zhu, P. Yu, F. Qi, G. Wang, X. Du, L. Bao, W. Deng, H. Zhu, J. Liu, J. Nie, Y. Zheng, H. Liang, R. Liu, S. Gong, H. Xu, A. Yisimayi, C. Qin, Structurally resolved SARS-CoV-2 antibody shows high efficacy in severely infected hamsters and provides a potent cocktail pairing strategy, *Cell* **183**, 1-11 (2020).
2. 3. G. De Luca, G. Cavalli, C. Campochiaro, E. Della-Torre, P. Angelillo, A. Tomelleri, N. Boffini, S. Tentori, F. Mette, N. Farina, P. Rovere-Querini, A. Ruggeri, T. D'Aliberti, P. Scarpellini, G. Landoni, F. De Cobelli, J. F. Paolini, A. Zangrillo, M. Tresoldi, B. C. Trapnell, F. Ciceri, L. Dagna, Gm-csf blockade with mavrilimumab in severe covid-19 pneumonia and systemic hyperinflammation: a single-centre, prospective cohort study. *The Lancet Rheumatology* **2**, e465-e467 (2020).
3. 4. Y. Wang, D. Zhang, G. Du, R. Du, J. Zhao, Y. Jin, S. Fu, L. Gao, Z. Cheng, Q. Lu, Y. Hu, G. Luo, K. Wang, Y. Lu, H. Li, S. Wang, S. Ruan, C. Yang, C. Mei, Y. Wang, D. Ding, F. Wu, X. Tang, X. Ye, Y. Ye, B. Liu, J. Yang, W. Yin, A. Wang, G. Fan, F. Zhou, Z. Liu, X. Gu, J. Xu, L. Shang, Y. Zhang, L. Cao, T. Guo, Y. Wan, H. Qin, Y. Jiang, T. Jaki, F. G. Hayden, P. W. Horby, B. Cao, C. Wang, Remdesivir in adults with severe COVID-19: a randomised, double-blind, placebo-controlled, multicentre trial, *The Lancet* **395**, 1569-1578 (2020).
4. 5. Y. Cao, J. Wei, L. Zou, T. Jiang, G. Wang, L. Chen, L. Huang, F. Meng, L. Huang, N. Wang, X. Zhou, H. Luo, Z. Mao, X. Chen, J. Xie, J. Liu, H. Cheng, J. Zhao, G. Huang, W. Wang, J. Zhou, Ruxolitinib in treatment of severe coronavirus disease 2019 (COVID-19): A multicenter, single-blind, randomized controlled trial. *J. Allergy Clin. Immunol.* **146,** 137-146 (2020).
5. 6. A. Pizzorno, B. Padey, T. Julien, S. Trouillet-Assant, A. Traversier, E. Errazuriz-Cerda, J. Fouret, J. Dubois, A. Gaymard, F. X. Lescure, V. Duliere, P. Brun, S. Constant, J. Poissy, B. Lina, Y. Yazdanpanah, O. Terrier, M. Rosa-Calatrava, Characterization and treatment of SARS-CoV-2 in nasal and bronchial human airway epithelia. *Cell Rep. Med.* **1**, 100059 (2020).
6. 7. M. Roschewski, M. S. Lionakis, J. P. Sharman, J. Roswarski, A. Goy, M. A. Monticelli, M. Roshon, S. H. Wrzesinski, J. V. Desai, M. A. Zarakas, J. Collen, K. M. Rose, A. Hamdy, R. Izumi, G. W. Wright, K. K. Chung, J. Baselga, L. M. Staudt, W. H. Wilson, Inhibition of Bruton tyrosine kinase in patients with severe COVID-19, *Science Immunol*. **5**, eabd0110 (2020).
7. 8. J. H. Beigel, K. M. Tomashek, L. E. Dodd, A. K. Mehta, B. S. Zingman, A. C. Kalil, E. Hohmann, H. Chu, A. Luetkemeyer, S. Kline, D. Lopez de Castilla, R.W. Finberg, K. Dierberg, V. Tapson, L. Hsieh, T.F. Patterson, R. Paredes, D.A. Sweeney, W.R. Short, G. Touloumi, D.C. Lye, N. Ohmagari, M. Oh, G.M. Ruiz-Palacios, T. Benfield, G. Fätkenheuer, M.G. Kortepeter, R. L. Atmar, C .B. Creech, J. Lundgren, A. G. Babiker, S. Pett, J. D. Neaton, T. H. Burgess, T. Bonnett, M. Green, M. Makowski, A. Osinusi, S. Nayak, H. C. Lane, Remdesivir for the treatment of Covid-19 — preliminary report, *N. Engl. J. Med.* DOI: 10.1056/NJEMoa2007764 (2020).
8. 9. Z. Jin, X. Du, Y. Xu, Y. Deng, M. Liu, Y. Zhao, B. Zhang, X. Li, L. Zhang, C. Peng, Y. Duan, J. Yu, L. Wang, K. Yang, F. Liu, R. Jiang, X. Yang, T. You, X. Liu, X. Yang, F. Bai, H. Liu, X. Liu, L. W. Guddat, W. Xu, G. Xiao, C. Qin, Z. Shi, H. Jiang, Z. Rao, H. Yang, Structure of Mpro from SARS-CoV-2 and discovery of its inhibitors, *Nature* **582**, 289–293 (2020).
9. 10. L. Zhang, D. Lin, X. Sun, U. Curth, C. Drosten, L. Sauerhering, S. Becker, K. Rox, R. Hilgenfeld, Crystal structure of SARS-CoV-2 main protease provides a basis for design of improved α-ketoamide inhibitors, *Science* **368**, 409-412 (2020).
10. 11. A. E. Finkelstein, D. T. Walz, V. Batista, M. Mizraji, F. Roisman, A. Minsher, Auranofin. New oral gold compound for treatment of rheumatoid arthritis, *Ann. Rheum. Dis.* **35**, 251-257 (1976).
11. 12. J. R. Ward, H. J. Williams, M. J. Egger, J. C. Reading, E. Boyce, M. Altz-Smith, CO. J. Samuelson , R. F. Willkens, M. A. Solsky, S. P. Hayes, K. L. Blocka, A.Weinstein, R. F. Meenan, M.Guttadauria, S. B. Kaplan, J. Klippel, Comparison of auranofin, gold sodium thiomalate, and placebo in the treatment of rheumatoid arthritis, *Arthritis Rheu.* **26**, 1303-1315 (1983).
12. 13. W. F. Kean, L. Hart, W. W. Buchanan, Auranofin, *Br. J. Rheumatol*. **36**, 560–572 (1997).
13. 14. F. Gao, Q. Yuan, P. Cai, L. Gao, L. Zhao, M. Liu, Y. Yao, Z. Chai, X. Gao, Au clusters treat rheumatoid arthritis with uniquely reversing cartilage/bone destruction, *Adv. Sci.* **6**, 1801671 (2019).
14. 15. Q. Yuan, F. Gao, Y. Yao, P. Cai, X. Zhang, J. Yuan, K. Hou, L. Gao, X. Ren, X. Gao, Gold clusters prevent inflammation-induced bone erosion through inhibiting the activation of NF-κB pathway, *Theranostics* **9**, 1825-1836 (2019).
15. 16. Cerner Multum, https://www.drugs.com/mtm/auranofin.html (2019).
16. 17. T. K. Rudolph, B. A. Freeman, Transduction of redox signaling by electrophile-protein reactions, *Science Signaling* **2**, re7 (2009).
17. 18. Q. Yuan, Y. Zhao, P. Cai, Z. He, F. Gao, J. Zhang, X. Gao, Dose-dependent efficacy of gold clusters on

rheumatoid arthritis therapy, *ACS Omega* **4**, 14092-14099 (2019).

18. 19. V. Grum-Tokars, K. Ratia, A. Begaye, S. C. Baker, A. D. Mesecar, Evaluating the 3C-like protease activity of SARS-Coronavirus: Recommendations for standardized assays for drug discovery, *Virus Research* **133**, 63–73 (2008).
19. 20. H. A. Rothan, S. Stone, J. Natekar, P. Kumari, K. Arora, M. Kumar, The FDA-approved gold drug Auranofin inhibits novel coronavirus (SARS-COV-2) replication and attenuates inflammation in human cells, *Virology* **547**, 7-11 (2020).
20. 21. J. Major, S. Crotta, M. Llorian, T. M. McCabe, H. H. Gad, S. L. Priestnall, R. Hartmann, A. Wack, Type I and III interferons disrupt lung epithelial repair during recovery from viral infection, *Science*, ***369***, 712-717 (2020).
21. 22. M. Catanzaro, F. Fagiani, M. Racchi, E. Corsini, S. Govoni, C. Lanni, Immune response in COVID-19: addressing a pharmacological challenge by targeting pathways triggered by SARS-CoV-2, *Signal Transduct. Target. Ther.* **5**, 84 (2020).
22. 23. M. Z. Tay, C. M. Poh, L. Renia, P. A. MacAry, L. F. P. Ng, The trinity of COVID-19: immunity, inflammation and intervention, *Nat. Rev. Immunol*. **20**, 363–374 (2020).
23. 24. Miriam Merad *et al*. Pathological inflammation in patients with COVID-19: a key role for monocytes and macrophages, *Nat. Rev. Immunol*. **20**, 355-362 (2020).
24. 25. G. Schett, B. Manger, D. Simon, R. Caporali, COVID-19 revisiting inflammatory pathways of arthritis, *Nat. Rev. Rheumatol.* **16**, 465-470 (2020)
25. 26. Cayman Chemical, Safety data sheet of Auranofin, https://www.caymanchem.com/msdss/15316m.pdf (2018).
26. 27. J. Sun, Z. Zhuang, J. Zheng, K. Li, R. L. Wong, D. Liu, J. Huang, J. He, A. Zhu, J. Zhao, X. Li, Y. Xi, R. Chen, A. N. Alshukairi, Z. Chen, Z. Zhang, C. Chen, X. Huang, F. Li, X. Lai, D. Chen, L. Wen, J. Zhuo, Y. Zhang, Y. Wang, S. Huang, J. Dai, Y. Shi, K. Zheng, M. R. Leidinger, J. Chen, Y. Li, N. Zhong, D. K. Meyerholz, P. B. McCray, Jr., S. Perlman, J. Zhao, Generation of a broadly useful model for COVID-19 pathogenesis, vaccination, and treatment, *Cell* **182**, 734-743 (2020).
27. A. Debnath, D. Parsonage, R. M. Andrade, C. He, E. R. Cobo, K. Hirata, S. Chen, G. Garcia-Rivera, E. Orozco, M. B. Martinez, S. S. Gunatilleke, A. M. Barrios, M. R. Arkin, L. B. Poole, J. H. McKerrow, S. L. Reed, A high-throughput drug screen for Entamoeba histolytica identifies a new lead and target, *Nat. Med.* **18**, 956–960 (2012).

Acknowledgments:

We thanks Dr. Feng Wang (Wuxi Biortus Bioscience Co. Ltd, 6 Dongsheng West Road, Jiangyin 214437, China) provide the gift plasmid for expression SARS-CoV-2 M^{pro}. We thank the staff from beamlines BL17U1, BL18U1 and BL19U1 at the Shanghai Synchrotron Radiation Facility for X-ray data collection. This work was supported by grants from National Natural Science Foundation of China (21727817, 11621505). Author contributions: X. G. conceived the project; H. Z., C. Z., Z. D., W. Z., Y. G., Y. Q., F. G. performed cell studies and enzyme activity; J. F., B. H., P.C., B.S. performed the sample preparation, characterization and data collection; X. G., X. G. performed theory calculation; Y. D., J. Q., and H. J. processed data analysis; W.T., F. Y., J. Z. performed animal studies; Y. G. and X. G. wrote the manuscript; all authors discussed and commented on the results and the manuscript.

Supplementary Materials:

Materials and Methods

Figures S1-S6

Tables S1-S2

References (1-8)

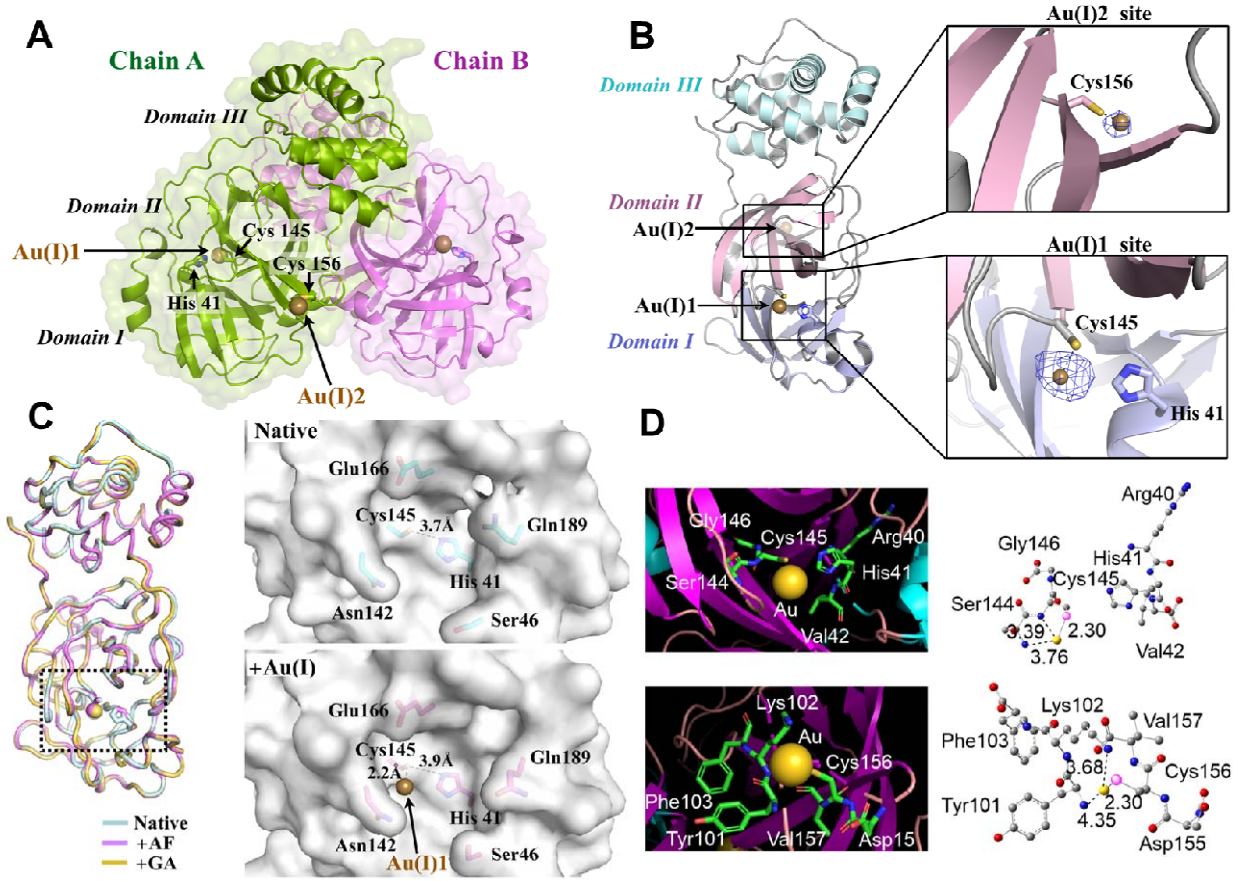

Fig. 1. The X-ray crystal structure of gold compounds treated M^{pro} in Au-S bound state. (**A**) The cartoon and surface presentation of M^{pro} homodimer in Au-S bound state with Chain A and Chain B colored in green and violet, respectively. (**B**) The cartoon presentation of one M^{pro} monomer with Domain I-III colored in light blue, light pink and pale cyan. Right images, The enlarged views of the Au(I)-S bound sites. The anomalous difference Fourier maps (blue mesh, contoured at 5 sigma) are shown for Au(I) 2 and Au(I) 1. The residues His41, Cys145 and Cys156 are shown in sticks and two Au(I) ions are shown in spheres. (**C**) Comparison of Au(I)-S bound state with the native state of M^{pro}. Superposition of crystal structures of AF treated (purple), GA treated (yellow) and untreated M^{pro} (blue). Right images, the catalytic pocket of native and Au(I)-S bound M^{pro} in surface presentation and the surrounding residues shown in sticks. For observation of Au(I)-Cys156 interaction, see Figure S4. (**D**) DFT calculation of interaction between Au(I) ions and Cys145 and Cys156 of M^{pro}, respectively. Left images show protein binding pockets consisting of amino acids and one Au(I) ions. Right images showed geometrically relaxed structures for the binding pockets encapsulating the Au(I), all Au−N atomic distances (in Å) within 5 Å are labeled with the corresponding distances obtained from the experimental crystal structure given in parentheses for comparison. C, N, O, S, and Au atoms are displayed in grey, blue, red, pink, and yellow colors, respectively. All H atoms are not shown for clarity.

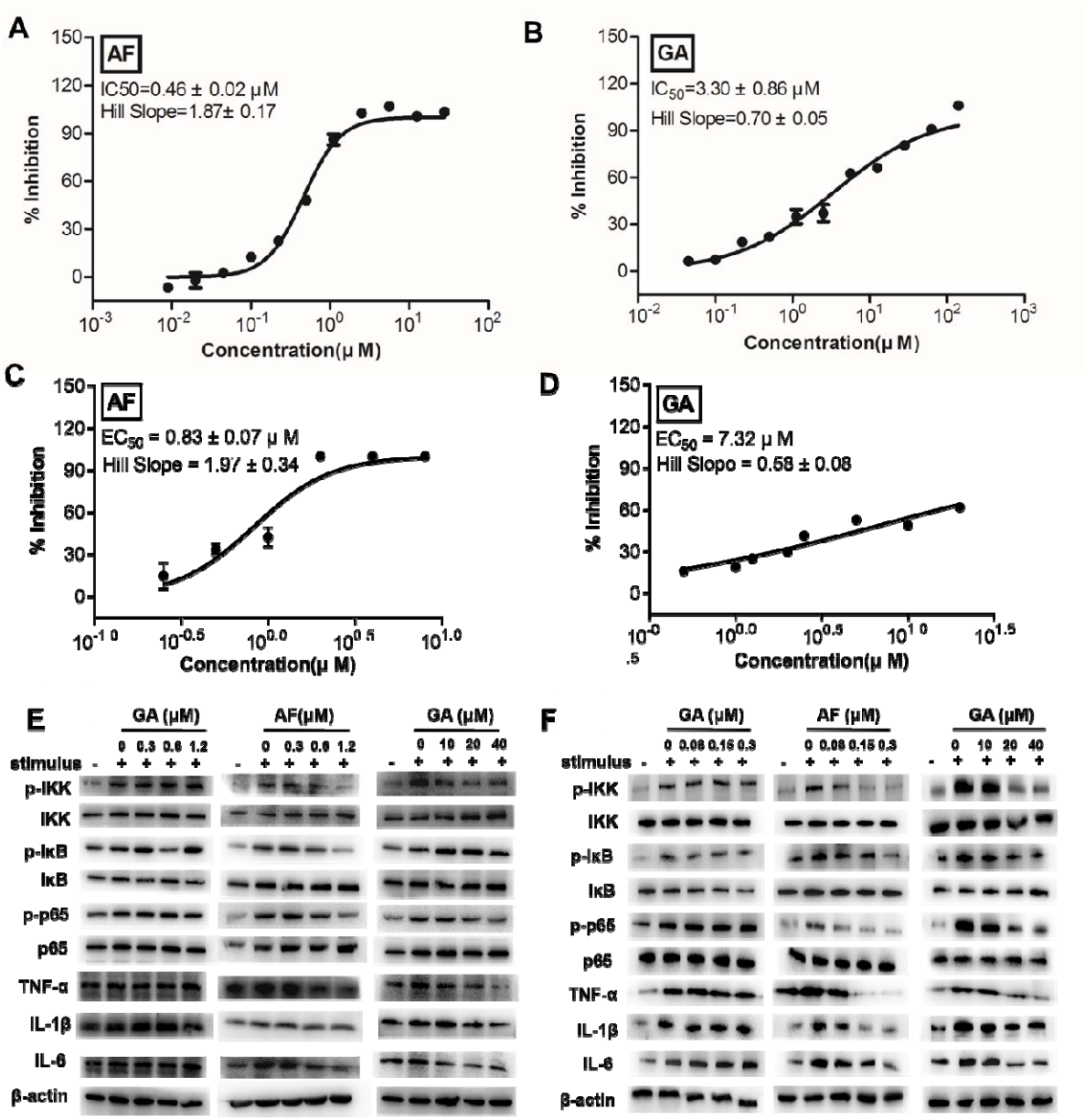

Fig. 2. AF or GA inhibit M^{pro} activity, suppress SARS-CoV-2 replication, and inactivate the NFκB pathway and suppress inflammatory cytokine expression in cells. (**A**) IC50 of AF. (**B**) The IC50 of GA. (**C**) EC50 of AF. (**D**) EC50 of GA. (**E**) For macrophages, low dose of AF (1.2μM) and high dose of GA (40 μM) significantly down-regulated NFκB activity and inhibit IL-6, IL-1β, TNF-α inflammation cytokine expression. (**F**) For human bronchial epithelial cell, low dose of AF (0.15 μM) and high dose of GA (20 μM) significantly reduce phosphorylation level of IKK, IκB, and p65 to suppress NFκB activation, thus inhibit IL-6, IL-1β, TNF-α inflammatory cytokine expression.

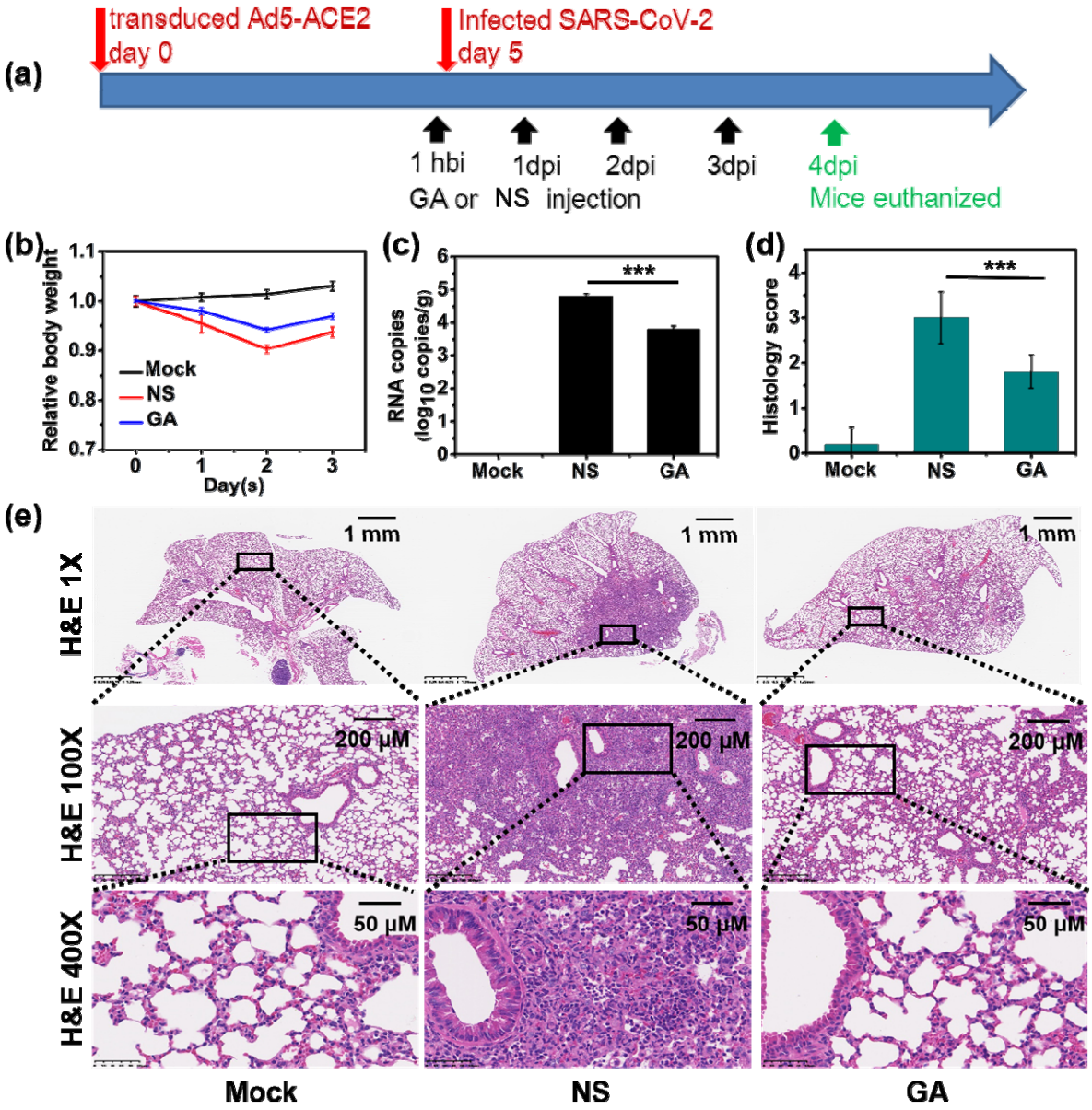

Fig. 3. The GA or NS treatment of COVID-19 mice. (**A**) The schematic diagram of GA or NS treated COVID-19 mice model. (**B**) The body weight loss of infected mice treated by GA or NS. (**C**) The virus RNA copies in lungs of mice at day 4 (unpaired t-test, ***p < 0.001). (**D**) Representative Hematoxylin-eosin (HE) staining of lungs from BALB/c mice harvested at the indicated time. (E) Histological scores of lung inflammation in SARS-CoV-2 infected mice.

Table 1. Animal acute toxicity and cytotoxicity of GA and AF

Animal/cell	Gold compounds	
	GA	AF
BALB/c Mice	LD50 >1000 mg/kg.bw	LD50 ~33.8 mg/kg.bw
SD Rat	LD50 ~288 mg/kg.bw	LD50 ~25 mg/kg.bw
epithelial cell	CC50 >100μM	CC50 ~0.6μM
Vero cell	CC50 >100μM	CC50 ~2.2μM
macrophage	CC50 >100μM	CC50 ~ 2.4μM

Table 2. Distribution of Au in mice tissue

Tissue	Concentration (μg/g)
plasma	15.01±0.30
brain	2.52±0.90
heart	10.3± 3.0
lung	51.07± 10
spleen	292.7± 12
liver	312.7±7.0
Spleen	624±2.70

Table 3. The pharmacokinetics of GA in SD Rat

parameter	unit	value	
		ip01（Female）	ip02（Male）
$AUC_{(0-t)}$	mg/L*h	533.680	509.615
$AUC_{(0-\infty)}$	mg/L*h	599.607	785.906
$A\mu MC_{(0-t)}$		6371.497	7609.285
$A\mu MC_{(0-\infty)}$		9797.793	26177.773
$MRT_{(0-t)}$	h	11.939	14.931
$MRT_{(0-\infty)}$	h	16.340	33.309
$VRT_{(0-t)}$	h^2	83.183	123.090
$VRT_{(0-\infty)}$	h^2	258.916	1045.121
$t_{1/2z}$	h	11.068	21.626
T_{max}	h	2	2
CL_z/F	L/h/kg	0.008	0.006
V_z/F	L/kg	0.133	0.199
C_{max}	mg/L	31.750	29.990
F	%	96.407	92.060

Supplementary Materials

Materials and Methods:

Molecular formula of AF and GA

The molecular formula of GA is $Au_{29}SG_{27}$ with a molecular weight of 13, 983 Da, single GA is composed of 28 Au atom and 27 glutathione molecules (see reference 14 in manuscript for detailed information). The molecular formula of AF is $C_{20}H_{35}AuO_9PS$ with a molecular weight of 679 Da.

Cloning, expression and purification of SARS-CoV-2 M^{pro} in E. coil

The full-length gene encoding SARS-CoV-2 M^{pro} was optimized and synthesized for Escherichia coli (E. coil) expression (GENEWIZ). Then the gene was cloned into a modified pET-28a expression vector with an N-terminal (His)6-tag followed by a Tobacco etch virus (TEV) cleavage site. The construct was confirmed by DNA sequencing. The plasmid was further isolated and transformed into the Escherichia coli Rosetta (DE3) expression strain (Invitrogen). The cells containing the plasmids above were grown to an OD600 of 0.8 and induced with isopropyl b-D-thiogalactopyranoside (IPTG) to a final concentration of 0.5mM at 16 ℃ for 14 h. Cells were then harvested by centrifugation at 4600g, resuspended in lysis buffer (l20mM Tris/HCl, pH 8.0, 20 mM imidazole and 300 mM NaCl) and lysed by French press, the lysate was centrifuged at 15 000 g for 50 min. Then the supernatant was loaded on to a Ni-NTA column pre-equilibrated with lysis buffer, and washed with 20 mM Tris/HCl, pH 8.0, 300 mM NaCl and 50 mM imidazole. The protein was eluted in 20 mM Tris/HCl, pH 8.0, 150 mM NaCl and 300 mM imidazole. TEV protease was added to the His tag fused protein and dialyzed overnight into anion-exchange chromatography buffer A（20mM Tris/HCl, pH8.0, 20mM NaCl, 1mM DTT, 1mM EDTA. The protein was further purified using a Resource-Q column of AKTA fast protein liquid chromatography (GE Healthcare) by elution with a linear gradient of 20-500 mM NaCl ,20 mM Tris/HCl，1mM EDTA，1mM DTT and pH 8.0. The purity was analysed by SDS/PAGE at each step. The purified and concentrated SARS-CoV-2 M^{pro} was stored in 20mM Tris-HCl (pH7.3), 20mM NaCl, 1mM DTT, 1mM EDTA for enzyme activity assays and crystallization.

LC-MASS studies of native M^{pro}

In brief, 5 μl of puried M^{pro} were applied in following studies. Liquid chromatography–mass spectrometry analyses were performed in positive-ion mode with a quadrupole-time-of-flight mass spectrometer combined with a high-performance liquid chromatograph for detecting the molecular weight of native M^{pro} Mass deconvolution was performed using Agilent MassHunter Qualitative Analysis B.06.00 software with BioConfirm Workflow.

Crystallization, data collection and structure determination

M^{pro} crystallization screening was carried out at 22 ℃ using the sitting-drop vapor-diffusion technique that 0.7μl 6mg/ml protein solution mixed with an equal volume of reservoir solution. Initial crystals were found under the crystallization conditions of the PEG/Ion Screen Kit in Crystal Screen (Hampton Research). After optimization, the best crystals of M^{pro} were obtained

under the condition of 200mM KF and 15% PEG 3350 after 4–5 d. Crystals of M^{pro} were soaked in reservoir solutions plus 10mM AF or GA respectively for over 15hr.
Prior to data collection, all crystals were cryo-protected by plunging them into a drop of reservoir solution supplemented with 10–20% glycerol, then flash frozen in liquid nitrogen. The diffraction data were collected at the beamlines in Shanghai Synchrotron Radiation Facility and were processed using softwares HKL3000 (1) or XDS (2).
The initial phase was determined by molecular replacement method using the program Phaser from CCP4 program suit (3), with the crystal structure of SARS-CoV-2 main protease M^{pro} in complex with an inhibitor N3 (PDB entry 6LU7) as the initial model (4). The refinement was carried out using Phenix (5) and Refmac (6), model building was carried out by COOT (7), and MolProbity (8) was used to validate the structure. The locations of Au (I) ions were identified according to the anomalous difference Fourier maps. Data collection and refinement statistics are listed in Table S1. The structural figures were prepared using PyMOL (http://www.pymol.org).

DFT Computation of Au(I)-M^{pro} binding energy.
The interaction energies between Au and M^{pro} protein were calculated by density functional theory (DFT) calculations. According to its crystal structure (**Figure 1** in manuscript), the protein has two binding pockets for Au and each encapsulates an Au atom (**Figure 1** in manuscript). The two Au atoms are binding with the S atoms of Cys145 and Cys156, respectively. To simulate the chemical environment of Au atoms, the residues within 5 Å from the Au atoms were considered. Specifically, Ser144, Cys145, Gly146, Arg40, His41, and Val42 in the first pocket (**Figure 1D**) and Tyr101, Lys102, Phe103, Asp155, Cys156 and Val157 in the second pocket (**Figure 1D**) were considered. There are four peptide bonds in each pocket. To maintain the skeleton structures of the two pockets, positions of C and N atoms of the peptide bonds were fixed and all the other atomic positions were allowed to be relaxed during the geometry optimizations. The B3LYP functional in conjunction with the SDD basis set for Au and the 6-31G(d,p) for nonmetal atoms were applied. The SDD pseudopotential was also applied for Au. During geometry optimizations, SMD solvation model was utilized to model the water environment. All the calculations were carried out using Gaussian 09 package.
The bond dissociation energy (E_{BD}) between Au and the protein binding pockets was calculated using the following equation,
$E_{BD} = E_{Au} + E_{ligands} - E_{complex}$
where E_{Au}, $E_{ligands}$, and $E_{complex}$ were the total energies of the complex, ligands of the pocket, and Au atom, respectively. $E_{ligands}$ was obtained by single-point energy calculation based on the optimized geometries of complexes with Au atom removed.
DFT calculations confirmed that Au atoms preferred to form S−Au bonds with the thiol groups (Cys145 in **Figure 1D** and Cys156 in **Figure 1D**) of the protein binding pockets, in agreement with **Figure 1** in manuscript. In addition, the N atoms of Ser144 and Cys145 (**Figure 1D**) and those of Tyr101 and Lys102 (**Figure 1D**) have distances within 5 Å from the corresponding Au atoms, suggesting the considerable electrostatic interactions between N and Au atoms. The bond dissociation energies (E_{BD}'s) between Au and the two pockets are 46.1 kcal mol−1 and 26.5 kcal mol^{-1}, respectively. Such large E_{BD}'s suggest that the Au atoms are firmly locked the pockets, which may efficiently inhibit the protein activity.

IC50 of gold compounds for M^{pro}

When the Auranofin or gold cluster was added into the enzymatic reaction solution, the change of initial rates was measured to evaluate their inhibitory effect. The gold molecule inhibit M^{pro} activity reaction mixture included 0.5 μM M^{pro} protein, 20 μM substrate (EDNAS-Glu)-Ser-Ala-Thr-Leu-Gln-Ser-Gly-Leu-Ala-(Lys-DABCYL)-Ser) (ChinaPeptides Co.,Ltd, Suzhou) and molecules from aforementioned gold compound. IC50 values of two gold compounds were measured using 0.5 μM protein, 20 μM substrate and 11 different inhibitor concentrations of compounds, respectively. Fluorescence intensity was monitored by the multimode plate reader (Bio-rad), excitation at 340nm and emission at 535nm. All experiments were performed in triplicate.

EC50 of gold compounds in Vero cell

Experiments with SARS-CoV-2 were performed under biosafety level 3 (BSL-3) conditions at Chinese Center for Disease Control and Prevention, P. R. China. Vero cells were infected with SARS-CoV-2 at a multiplicity of infection (MOI) of 0.015 diluted in DMEM/F12 without FCS at 37°C for 1 h. Cells were washed with DMEM/F12 with 10% FCS and supplemented with auranofin or gold cluster in different concentrations. For solvent control, cells were only treated with 1% DMSO. 48 hours after infection (h.p.i.), cells supernatant were collected and virus RAN was subjected to qRT-PCR. All experiments were performed in triplicate.

Western blot analysis of NFκB and inflammatory cytokine in macrophage and bronchial epithelial cell

RAW 264.7 or 16HBE cell were seeded into 6 well plates at a density of 2×10^6cells/well. After incubation without or with TNFα (50ng mL^{-1}) and different concentration of auranofin or gold clusters for 24 h, the cells were collected and lysed with RIPA buffer (50 mmol L^{-1}Tris-HCl, pH 7.4, 150 mmol L^{-1} NaCl, 1% Triton X-100, 1% sodium deoxycholate, 0.1% SDS, 1 mmol L^{-1} sodium orthovanadate, 50 mmol L^{-1} NaF, and 1 mmol L^{-1}ethylenediaminetetraacetic acid) along with protease inhibitor (Roche Molecular Biochemicals). The lysate was centrifuged at 13 000 rpm for 10 min, and the supernatant was stored for subsequent analysis. The concentration of protein was determined using a microplate spectrophotometer (SpectraMax M4, Molecular Devices, USA) at a wavelength of 595 nm. An equal quantity of protein (50 μg) was separated by 10% SDS-PAGE and transferred to a polyvinylidene fluoride (PVDF) membrane (0.45 μm, Millipore, USA). After blocking, the membrane was incubated with specific antibodies for COX-2 (Cell Signaling Technologies, 12282, 1:1000), IL-1β (Cell Signaling Technologies, 12703, 1:1000), IL-6 (Cell Signaling Technologies, 12912, 1:1000), TNF-α (Cell Signaling Technologies, 11948, 1:1000), phosphor-p65 (Cell Signaling Technologies, 3033, 1:1000), p65 (Cell Signaling Technologies, 3034, 1:1000), phosphor-IκBα (Cell Signaling Technologies, 2859, 1:1000), IκBα (Cell Signaling Technologies, 4812, 1:1000), IKKα (Cell Signaling Technologies, 2682, 1:1000), IKKβ (Cell Signaling Technologies, 8943, 1:1000), phosphor-IKKα/β (Cell Signaling Technologies, 2697, 1:1000), followed by incubation with an appropriate secondary antibody conjugated to horseradish peroxidase (Beyotime Biotechnology, China).

Cell toxicity of gold compounds in Vero E6, RAW264.7 and 16HBE cell line

Serial dose of auranofin or gold cluster were added into cell culture media, respectively. After 48 hrs incubation with different cell line, cell viability was checked by CCK8 (Beyotime, China) following kits instruction, all studies were carried in triplicate. All cells were obtained from ATCC with authentication service.

The studies of mice LD50

100 adult female BALB/c mice for experiments were conducted in compliance with regulations of the National Act on the use of experimental animals (China) and were approved by the Institutional animal care and ethic committee at the Chinese Academy of Sciences (approved No. SYXK (jing) 2014-0023). Their weights ranged between (18g~22g). Mice were housed in plastic cages, each cage contained 10 mice. Animals were kept under controlled temperature of 25 ± 2 ^{o}C for12 hours under light and 12 hours dark cycle throughout the experiment. The LD50 was studied by a "staircase method" with increasing doses of GA. Ten doses of 100, 200, 300, 400, 500, 600, 700, 800, 900, 1000mg/kg b.wt., were given to 10 groups of mice (10 in each) for the determination of intraperitoneal LD50 in female mice. Animals were observed for the 2, 6, and 24 hours for any toxic symptoms. After 24 hours, number of died animals was counted in each group and LD50 determined by the method of Karber. In this study, none mice were dead within 24 hour after GA were injected.

The body weight loss, virus load in lung, and lung pathologic studies of GA treated COVID-19 mice

Virus and cells

Specific pathogen-free 6 week old female BALB/c mice were purchased from SiPeiFu Laboratory Animal Co (Beijing, China). All protocols were approved by the Institutional Animal Care and Use Committees of National, Institute for Viral Disease Control & Prevention, Chinese Center for Disease Control and Prevention. The SARS-CoV-2 strains used in this research were isolated from COVID-19 patient (BetaCoV/Wuhan/IVDC/-HB -01/2020, EPI_ISL_402119) and passaged on Vero cells. The human serotype 5 adenoviral vector expressing human ACE2 under the control of the CMV promoter was a gift kindly provided by Dr. Zhao Juncun.

Viral RNA extraction and RT-qPCR

Viral RNA was extracted from 100 μL supernatant of infected cells using the automated nucleic acid extraction system (TIANLONG, China), following the manufacturer's recommendations. SARS-COV-2 virus detection was performed using the One Step PrimeScript RT-PCR kit (TaKaRa, Japan) on the LightCycler 480 Real-Time PCR system (Roche, Rotkreuz, Switzerland). The following primers targeting ORF1a were used in the study:

Forward primer: 5□-AGAAGATTGGTTAGATGATGATAGT-3□;

Reverse primer: 5□-TTCCATCTCTAATTGAGGTTGAACC-3□;

Probe 5□-FAM-TCCTCACTGCCGTCTTGTTG ACCA-BHQ1-3□.

Transduction and infection of mice

COVID-19 mice generated as previously reported (reference 1 in manuscript), 12 mice were divided into 3 groups with four mice each, mice were anesthetized with pentasorbital sodium and transduced intranasally by 2.5×10^{8} FFU of Ad5-ACE2 in 50 μL DMEM. Five days post transduction, 1 h before infection, mice received a dose of 15 mg/kg GA intraperitoneal injection (i.p.) in a volume of 150 μL, an equivalent volume of NS was administered as a control. Then

mice were infected intranasally with SARS-CoV-2 (1×105 PFU) in a total volume of 50 μL DMEM. Mice received GA or NS i.p. treatment for three days. All mice were weighted at every day and euthanized at 4dpi. The lung homogenates were weighed and prepared in differential volume of NS (0.1 g tissue with 0.5 mL NS) and crushed for 10 min and then centrifuged at 3000 rpm for 10 min at 4 ℃. The 100 μL supernatant of lung homogenates were collected to extract viral RNA and qRT-PCR were used to assess the SARS-CoV-2 RNA copies.

Pathological Examination of mice

Animals were anesthetized and the lungs were fixed in 4% (v/v) paraformaldehyde solution for 48 hours, and the paraffin sections (3-4 μm) were prepared routinely. The paraffin sections were stained with Hematoxylin and Eosin (H&E) to identify histopathological changes in the lungs. The histopathology of the lung tissue was observed by light microscopy.

All work with SARS-CoV-2 was conducted in the Biosafety Level 3 (BSL3) Laboratories of National Institute for Viral Disease Control & Prevention, Chinese Center for Disease Control and Prevention.

Bio-distribution, side effects, and pharmacokinetics study of gold compounds in mice/rats

BALB/c female Mice and SD Rats for experiments conducted in compliance with regulations of the National Act on the use of experimental animals (China) and were approved by the Institutional animal care and ethic committee at the Chinese Academy of Sciences (approved No. SYXK (jing) 2014-0023). The mice were intraperitoneally injected at dose of 15mg/kg for 4 times (one time/day by 4 days). The 6 hours after the last GA injection, the mice were anesthetized and half of the organ were analysized by ICP-MASS to check the Au ingredient in blood, brain, heart, lung, liver, spleen, and kidney. Half of the main tissues were fixed in 4% (v/v) paraformaldehyde solution for 48 hours, and the paraffin sections (3-4 μm) were prepared routinely. The paraffin sections were stained with Hematoxylin and Eosin (H&E) to identify histopathological changes. The Au ingredient in half of organs were with ICP-MS (Thermo-X7). After intraperitoneal injection or intravenous injection of 5mg Au/kg.bw for male and female SD rat, respectively, bloods were collected from jugular vein at serial time point. The blood content of Au was analyzed with ICP-MS (Thermo-X7). PK parameters were determined using a non-compartmental analysis with PKSolver.

Supplementary references:

1. Minor, W., Cymborowski, M., Otwinowski, Z. & Chruszcz, M. HKL-3000: the integration of data reduction and structure solution - from diffraction images to an initial model in minutes. Acta Crystallographica Section D 62, 859-866 (2006).
2. Kabsch W (2010) XDS. Acta Crystallogr D Biol Crystallogr 66:125–132.
3. Potterton, L. et al. CCP4i2: the new graphical user interface to the CCP4 program suite. Acta Crystallographica Section D-Structural Biology 74, 68-84 (2018).
4. Jin Z , Du X , Xu Y , et al. Structure of Mpro from COVID-19 virus and discovery of its inhibitors. Nature, 2020, 582(7811):1-9.
5. Afonine, P. V. et al. Towards automated crystallographic structure refinement with phenix.refine. Acta crystallographica Section D-Structural Biology ,2012, 68, 352-367.
6. Murshudov, G. N. et al. REFMAC5 for the refinement of macromolecular crystal structures. Acta crystallographica. Section D, Biological crystallography 67, 355-367, doi:10.1107/S0907444911001314 (2011).
7. Emsley, P., Lohkamp, B., Scott, W. G. & Cowtan, K. Features and development of Coot. Acta 459 Crystallographica Section D: Biological Crystallography 66, 486-501 (2010).
8. Chen, V. B. et al. MolProbity: all-atom structure validation for macromolecular crystallography. Acta crystallographica. Section D, Biological crystallography 66, 12-21, doi:10.1107/S0907444909042073 (2010).

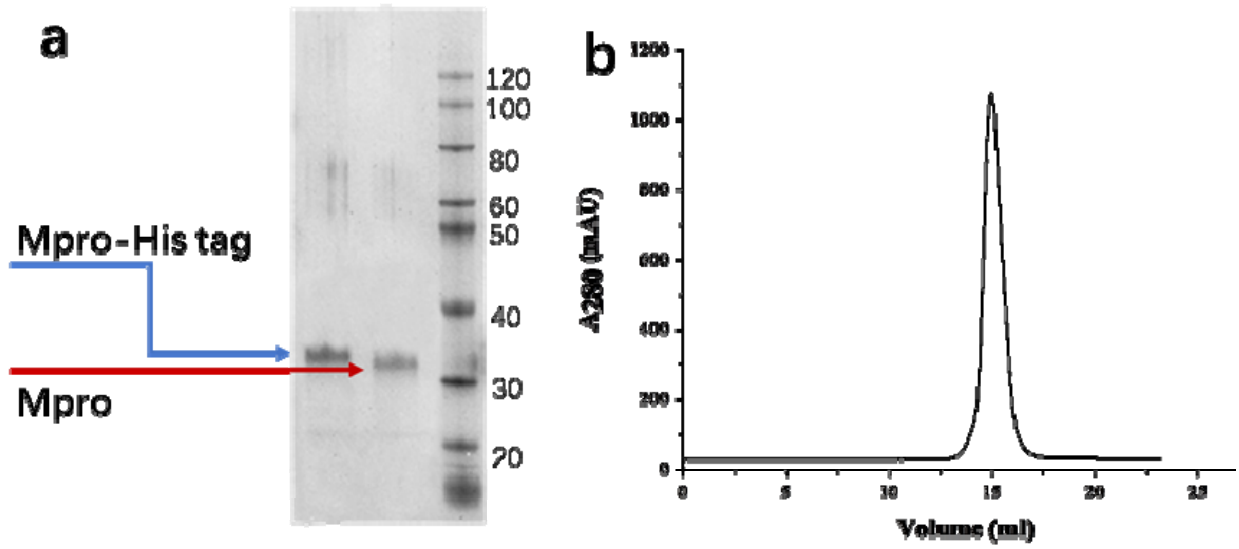

Figure S1. The purification of SARS-CoV-2 M^{pro}. (a), The SDS-PAGE gel of M^{pro}-His tag and M^{pro}. (b), Size-exclusion chromatography profile of native M^{pro}.

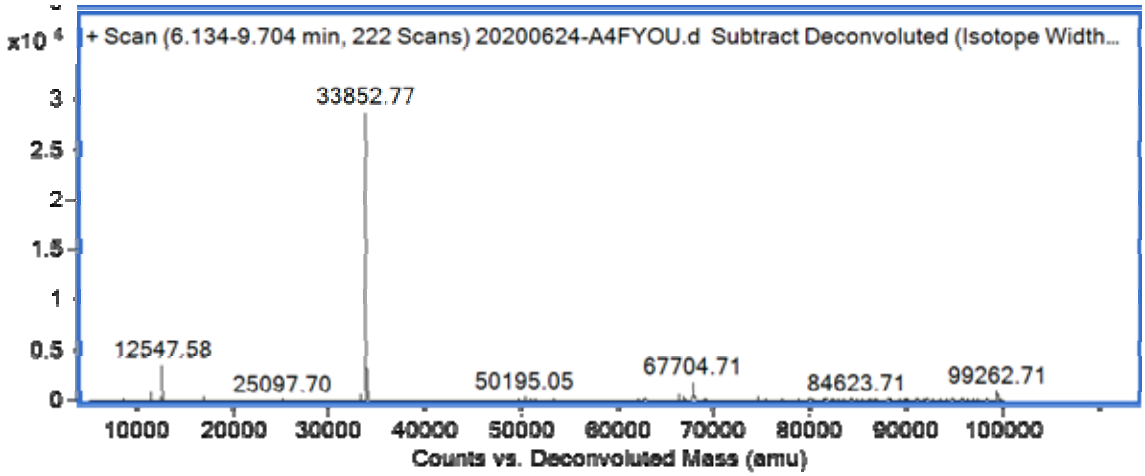

Figure S2. The mass spectra of native M^{pro}.

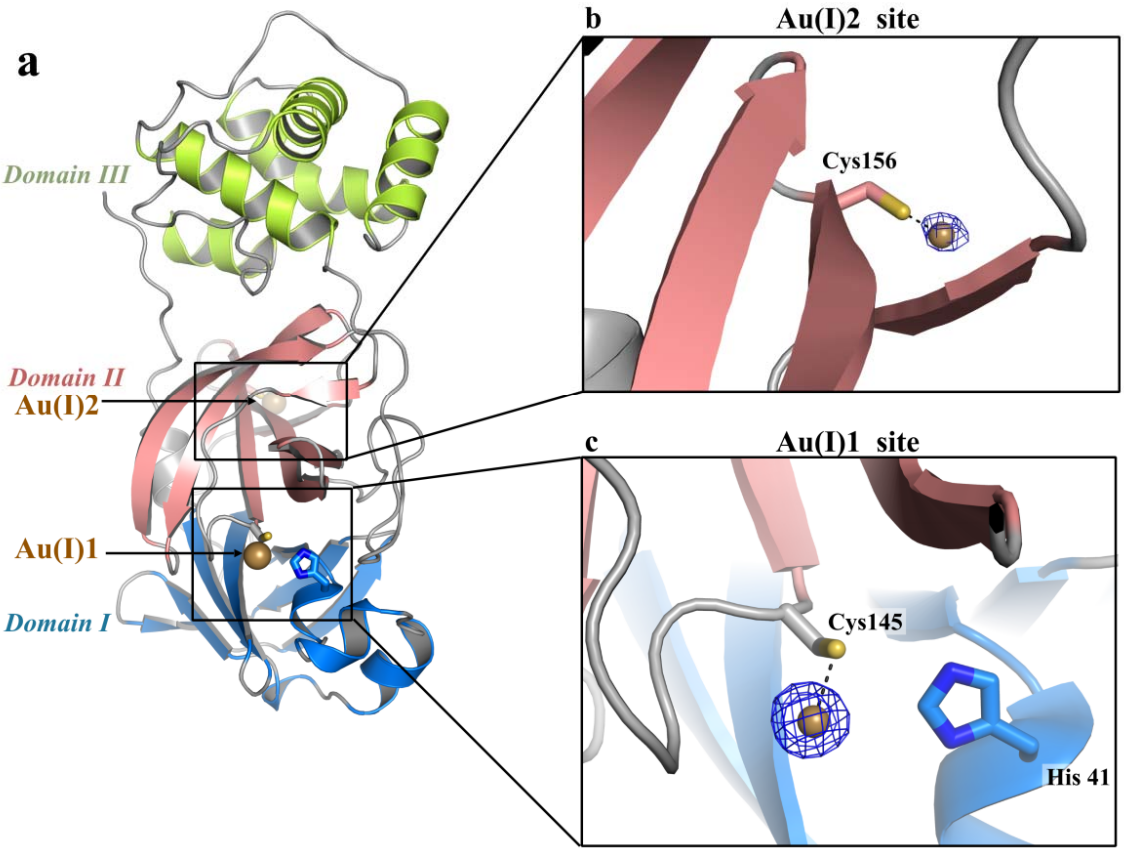

Figure S3. The structure of M^{pro} treated by GA. (a) The cartoon presentation of one M^{pro} monomer. (b, c) The enlarged views of the Au(I)-S bound sites. The anomalous difference Fourier maps (blue mesh) are shown for Au(I)2 (b) and Au(I)1 (c).

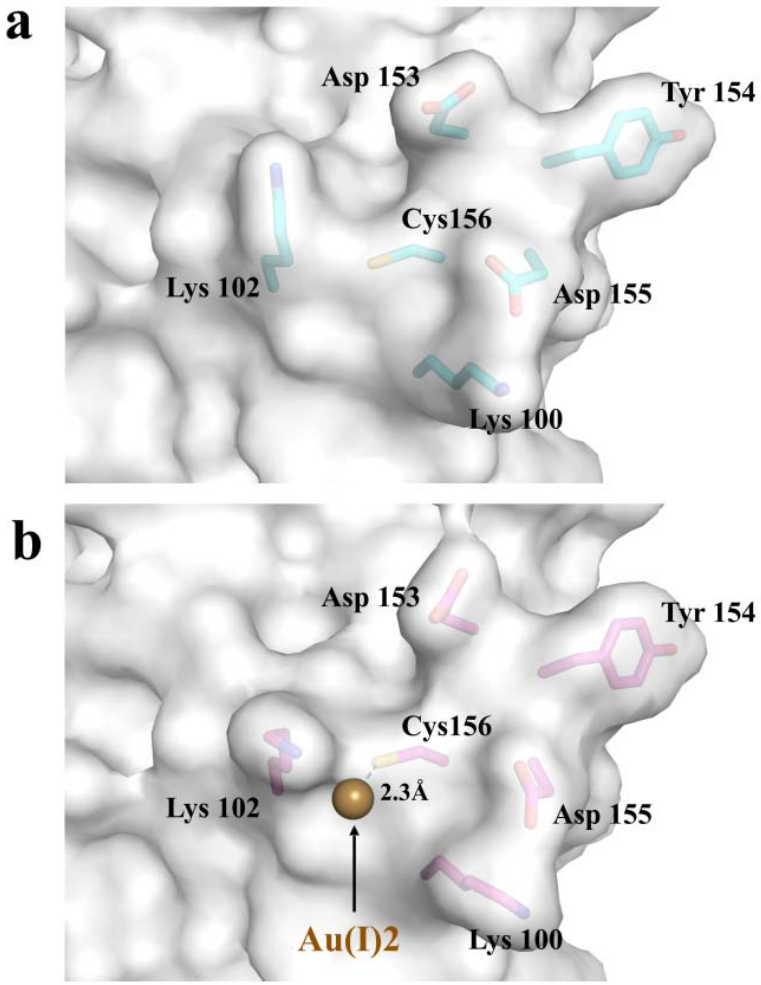

Figure S4. Comparison of Au(I) 2-binding pocket with native. (a) and Au(I)-S(Cys156) bound M^{pro} (b) in surface presentation and the surrounding residues shown in sticks.

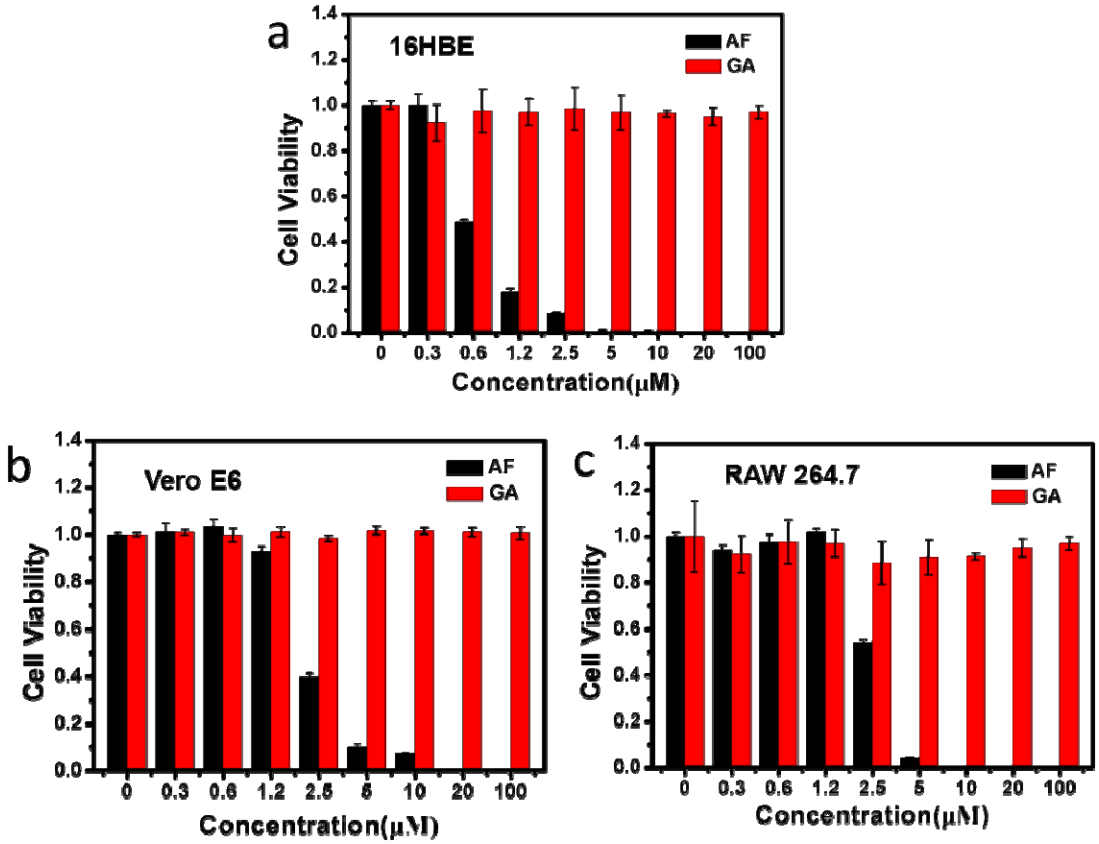

Figure S5. Cell viability of AF and GA. (a) 16HBE cell viability when cell exposed serial dose of AF or GA for 48 hrs, respectively. (b) Vero E6 viability when cell exposed serial dose of AF or GA for 48 hrs, respectively. (c) RAW264.7 cell viability when cell exposed serial dose of AF or GA for 48 hrs, respectively.

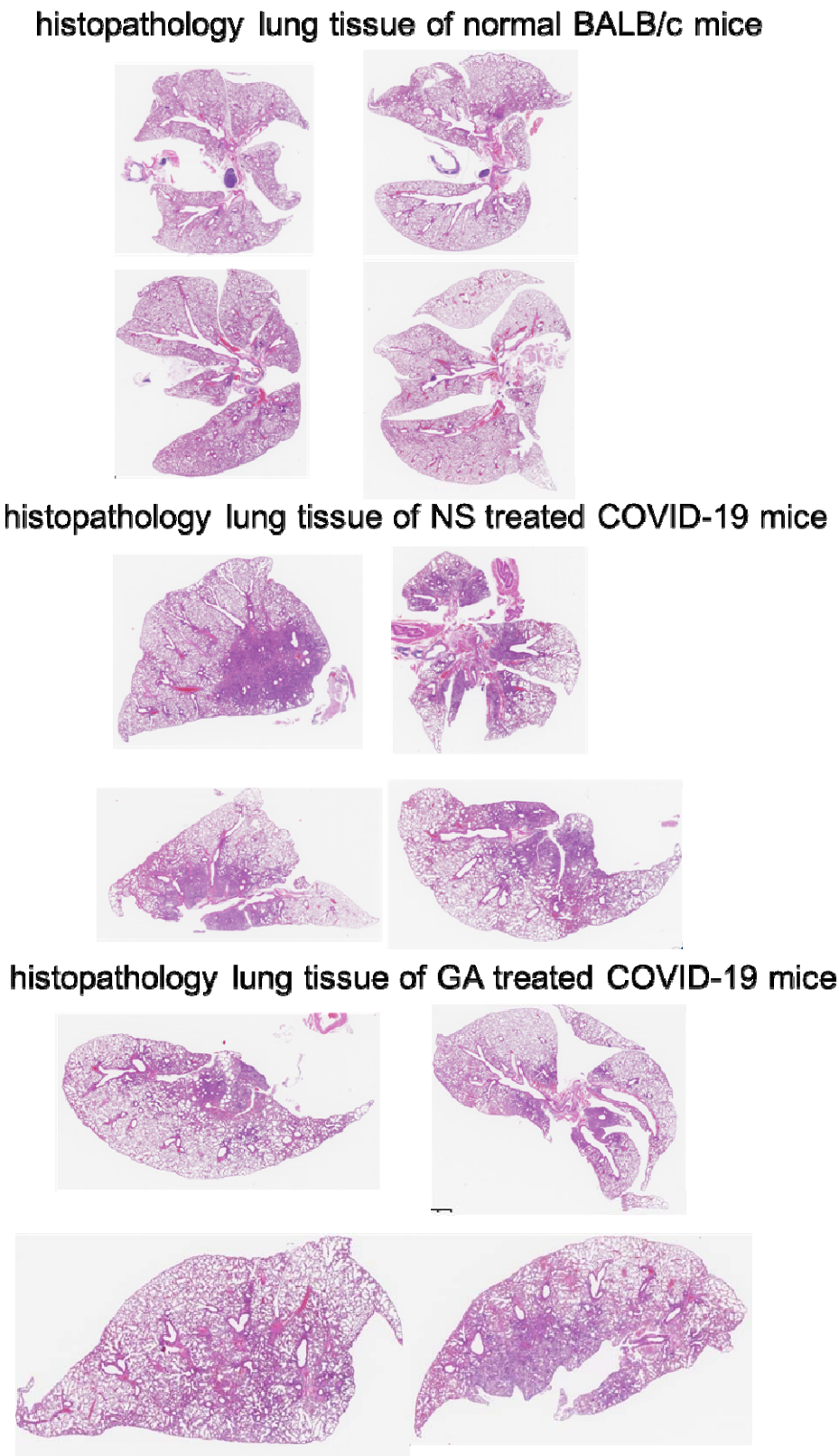

Figure S6. The lung sections of normal mice, NS treated mice, and GA treated mice.

Table 1. Data collection and refinement statistics

	M^{pro}-AF treated	M^{pro}-GA treated	M^{pro}-Native
Data collection			
Wavelength (Å)	0.86	0.98	0.98
Space group	C2	C2	C2
Cell dimensions			
a, *b*, *c* (Å)	114.3, 54.0, 44.7	113.8, 53.8, 44.6	113.9, 53.8, 44.7
α, β, γ (°)	90.0, 101.8, 90.0	90.0, 102.0, 90.0	90.0, 101.5, 90.0
Resolution (Å)	50-2.75 (2.90-2.75) [a]	50-1.72 (1.75-1.72) [a]	50-1.77 (1.80-1.77) [a]
R_{merge}	0.094 (0.154)	0.089 (0.823)	0.070 (0.542)
$\langle I/\sigma(I)\rangle$	14.0 (7.0)	33.8 (2.2)	24.3 (2.4)
Completeness (%)	96.4 (80.9)	99.8 (100.0)	99.3 (95.9)
Redundancy	5.4 (3.4)	6.2 (6.0)	6.6 (4.9)
Refinement			
Resolution (Å)	50-2.75	50-1.72	50-1.77
No. reflections	6,781	27,941	25,369
R_{work}/ R_{free}	0.196/0.230	0.199/0.237	0.209/0.254
No. atoms			
Protein	2,329	2,329	2,329
Au	2	2	0
Water	111	235	239
B-factors	34.8	37.8	23.5
Rmsd bond length (Å)	0.006	0.008	0.008
Rmsd bond angle (°)	1.0	1.0	1.0
Ramachandran Plot			
Favoured (%)	97.7	97.7	99.0
Allowed (%)	2.3	2.3	0.7
Outliers (%)	0	0	0.3

[a] The values in parenthesis mean those of the highest resolution shell.

Table S2. Rat Intravenous injection 5 mg/kg.bw of gold cluster

Parameters	Unit	Parameter value	
		iv 01（F）	iv 02（M）
$AUC_{(0-t)}$	mg/L*h	641.972	465.165
$AUC_{(0-\infty)}$	mg/L*h	823.672	556.880
$AUMC_{(0-t)}$		8616.252	5459.131
$AUMC_{(0-\infty)}$		19606.123	10532.811
$MRT_{(0-t)}$	h	13.422	11.736
$MRT_{(0-\infty)}$	h	23.803	18.914
$VRT_{(0-t)}$	h^2	110.213	91.859
$VRT_{(0-\infty)}$	h^2	598.942	399.534
$t_{1/2z}$	h	16.967	13.389
CL_z	L/h/kg	0.006	0.009
V_z	L/kg	0.149	0.173